PHOTOMASK

BACUS—The international technical group of SPIE dedicated to the advancement of photomask technology.

BACUS N • E • W • S

DECEMBER 2018
VOLUME 34, ISSUE 12

Best Student Poster Zeiss award — PUV18

Automated Rough Line Edge Estimation from SEM Images Using Deep Convolutional Neural Networks

Narendra Chaudhary, Serap A. Savari, and S.S. Yeddulapalli, Texas A&M University, Mail Stop 3128 TAMU, College Station, TX 77843-3128, USA

ABSTRACT

We propose a deep convolutional neural network named EDGENet to estimate rough line edge positions in lowdose scanning electron microscope (SEM) images corrupted by Poisson noise, Gaussian blur, edge effects and other instrument errors and apply our approach to the estimation of line edge roughness (LER) and line width roughness (LWR). Our method uses a supervised learning dataset of 100800 input-output pairs of simulated noisy SEM rough line images with true edge positions. The edges were constructed by the Thorsos method and have an underlying Palasantzas spectral model. The simulated SEM images were created using the ARTIMAGEN library developed at the National Institute of Standards and Technology. The convolutional neural network EDGENet consists of 17 convolutional, 16 batch-normalization layers and 16 dropout layers and offers excellent LER and LWR estimation as well as roughness spectrum estimation.

1. Introduction

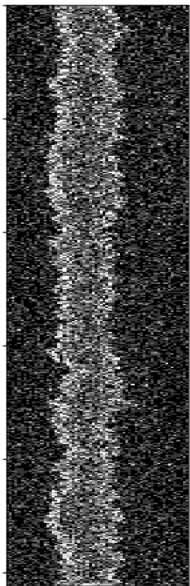

Figure 1. A noisy SEM image of dimension 64 x1024. The image has one line with two edges. The aspect ratio of the image has been scaled for a better view.

The measurement of line-edge roughness and line width roughness (LER, LWR) is necessary to understand and control semiconductor device performance and the yield of the manufacturing process. The scanning electron microscope (SEM) is often used for the roughness measurements. Low-dose SEM images are potentially attractive because of relatively small acquisition times and resist shrinkage. However, to determine the edge geometry from such images requires techniques to account for Poisson noise, Gaussian blur, edge effects and other instrument errors.[1,2] One could use algorithms based on filtering[3] ror physical model-based regression.[4,5] The filtering based methods often require careful selection of the filter parameters to prevent changes in the edge geometry while model-based regression is constrained by the modeling assumptions. Therefore, the algorithmic problems associated with the extraction of edge geometries in a high-volume manufacturing setting continue to be investigated.

While a single number is often used to characterize LER or LWR, that one number does not capture all interesting features of a rough edge or width.[6,7] The power spectral density (PSD) analysis of edge or line roughness offers more detailed information[6] and is useful for process monitoring[8,9] and understanding aspects of transistor performance.[10] It is difficult to accurately estimate the power spectrum of a rough edge or line from a low-dose SEM image because of the artifacts that corrupt those images.[6,7] Therefore, new techniques to automate the estimation of edge geometries and to improve the accuracy of power spectrum density estimates are potentially useful for semiconductor manufacturing.

We propose the use of deep convolutional neural networks (CNNs) as they have had widespread application[11] and success in image processing[12,13] and classification problems.[11,14] Motivated by the success of the DnCNN[12] blind Gaussian denoising algorithm on natural images, we recently introduced and showed the superiority of the convolutional neural network SEMNet[15] for the Poisson denoising of SEM rough line images with unknown noise levels; we used the Canny algorithm on the denoised image to complete the edge detection procedure.

TAKE A LOOK INSIDE:

INDUSTRY BRIEFS —see page 9

CALENDAR For a list of meetings —see page 10

SPIE.

10810-56

EDITORIAL

Addressing the bifurcation of the photomask industry

Peter Buck, Mentor Graphics

The combined conferences of Photomask Technology and EUV Lithography were held last month in Monterey, California. Attendance was about 10% higher than in 2017 at approximately 580 total attendees. This is a good number for the venue, the recently rebuilt Monterey Convention Center, and the conference felt just right – crowded enough to confirm that the conference was alive and well but not so crowded that a seat was impossible to obtain for someone entering the conference rooms late. The eBeam Initiative presented an optimistic overview of the mask industry business assessment with strong growth at all technology nodes. Behind the scenes, though, the picture was more complex. At the Steering Committee breakfast meeting we were confronted with the fact that the number of abstracts submitted to each of the two conferences continues its steady decline - 58% in the last decade. While the technical focus of the conference has been EUV lithography, a look at the abstract contributors reveals that of the six companies most likely to deploy EUV lithography, there were only seven abstracts submitted. Of these, six were submitted by GLOBALFOUNDRIES. Based on their publically announced decision to pivot away from 7nm it is unlikely we will see any EUV abstracts from GLOBALFOUNDRIES next year. This presents a challenge to the conference steering committee – how to continue to present a forum for advanced photomask technology even if the companies who need EUV to be successful do not participate, while in addition serving the broader industry needs.

Perhaps the answer is to rebalance the photomask portion of the conference towards the vast majority of photomasks that are not EUV. The eBeam Initiative survey showed that even without any input from TSMC, the total annual mask volume has increased to about 600,000 masks. Of that total only ~2200 were EUV masks. The segment of 130 nm and above grew by about 24,000 masks while the total number of laser writer produced masks increased by ~100,000. This industry is as healthy as it has ever been, to the extent that capacity is now a problem. In a talk at the eBeam Initiative reception Tuesday evening, Franklin Kalk of Toppan Photomasks projected a near-term mask writer equipment shortfall of up to 100 tools as equipment as old as 30 years finally goes out of service, while at the same time demand for photomasks continues to grow. The urgent need for new, cost efficient photomask manufacturing equipment at all levels of technology provides opportunities for technology innovation to meet these challenges for companies willing to think creatively. The Photomask Technology conference can continue to serve by adapting to the changing needs of our industry as it has done for over 30 years. The co-location and coordination of the Photomask Technology and EUV Lithography conferences provides an infrastructure to continue to support both advanced and mature technology needs as the photomask industry continues to expand both in depth and breadth. To be successful, WE – all of us – need to participate with contributions that break beyond the traditional bleeding edge of resolution! I look forward to seeing all of you at the 2019 conference.

BACUS N • E • W • S

BACUS News is published monthly by SPIE for BACUS, the international technical group of SPIE dedicated to the advancement of photomask technology.

Managing Editor/Graphics Linda DeLano
Advertising Melissa Farlow
BACUS Technical Group Manager Marilyn Gorsuch

■ 2018 BACUS Steering Committee ■

President
Jim N. Wiley, *ASML US, Inc.*

Vice-President
Frank E. Abboud, *Intel Corp.*

Secretary
Larry S. Zurbrick, *Keysight Technologies, Inc.*

Newsletter Editor
Artur Balasinski, *Cypress Semiconductor Corp.*

2018 Annual Photomask Conference Chairs
Emily Gallagher, *IMEC*
Jed Rankin, *GLOBALGOUNDRIES Inc.*

International Chair
Uwe F. W. Behringer, *UBC Microelectronics*

Education Chair
Frank E. Abboud, *Intel Corp.*

Members at Large
Michael D. Archuletta, *RAVE LLC*
Ki-ho Baik, *HOYA Corp. USA*
Peter D. Buck, *Mentor Graphics Corp.*
Brian Cha, *Samsung Electronics Co., Ltd.*
Derren Dunn, *IBM Corp.*
Thomas B. Faure, *GLOBALFOUNDRIES Inc.*
Aki Fujimura, *DS2, Inc.*
Brian J. Grenon, *Grenon Consulting*
Jon Haines, *Micron Technology Inc.*
Naoya Hayashi, *Dai Nippon Printing Co., Ltd.*
Bryan S. Kasprowicz, *Photronics, Inc.*
Patrick M. Martin, *Applied Materials, Inc.*
Kent Nakagawa, *Toppan Photomasks, Inc.*
Jan Hendrik Peters, *bmbg consult*
Moshe Preil, *KLA-Tencor Corp.*
Stephen P. Renwick, *Nikon Research Corp. of America*
Douglas J. Resnick, *Canon Nanotechnologies, Inc.*
Thomas Scheruebl, *Carl Zeiss SMT GmbH*
Thomas Struck, *Infineon Technologies AG*
Bala Thumma, *Synopsys, Inc.*
Anthony Vacca, *Automated Visual Inspection*
Michael Watt, *Shin-Etsu MicroSi Inc.*

SPIE.

P.O. Box 10, Bellingham, WA 98227-0010 USA
Tel: +1 360 676 3290
Fax: +1 360 647 1445
www.SPIE.org
help@spie.org

©2018

All rights reserved.

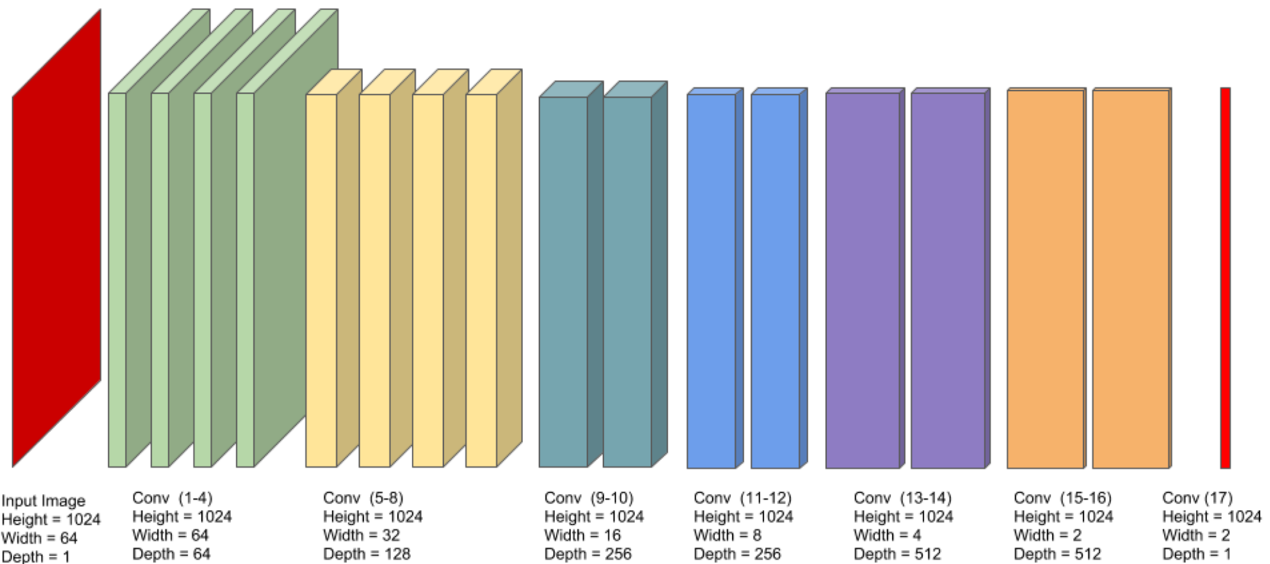

Figure 2. The 17 convolutional layers of EDGENet, which inputs a noisy SEM image of dimension 64x1024 and outputs a vector of dimension 2x1024.

Here we propose a new deep convolutional neural network named EDGENet which inputs a SEM rough line image corrupted by an unknown level of Poisson noise and directly outputs the estimated edge positions. EDGENet uses the same set of 100800 noisy line images as SEMNet15 for training and testing purposes. The edge dataset was created using the Thorsos method[16,17] with an underlying Palasantzas[18] spectral model and many combinations of parameters for LER, correlation length and roughness exponent. These edges were input to the SEM simulator ARTIMAGEN[19,20] to generate noisy images. EDGENet automatically learns to recognize the edge position in a variety of edge geometries and noise levels and provides excellent measurement accuracy.

The remainder of the paper is organized as follows. In Section 2, we discuss deep convolutional neural networks and the proposed EDGENet architecture. In Section 3, we discuss the dataset and the proposed methodology. In Section 4, we show the accuracy of LER/LWR estimation and edge spectra results. In Section 5, we conclude the paper.

2. Deep Convolutional Neural Networks

Machine learning has improved significantly in the last decade. Machine learning algorithms can be broadly classified as either unsupervised machine learning algorithms or supervised machine learning algorithms. Unsupervised machine learning algorithms find structure in the input data without a known or expected output. In supervised learning pairs of input-output data points are available and the objective is to find a relationship in the pairs. We developed EDGENet by using supervised machine learning.

Given a collection of N input-output vector pairs (X^i; Y^i) the first step in supervised machine learning is to choose a model or a parametric function $f(X)$ which is complex enough to describe the relationship between the input and output pairs. For example, a linear function with a variable weight matrix W and a bias vector b term has the form

$$f(X) = WX + b.$$

The next step is the selection of a performance criteria or a loss term, and two widely used criteria are the mean squared error (MSE) and the mean absolute error (MAE)

$$\mathrm{MSE} = \frac{1}{N} * \sum_{i=1}^{N} \|Y^i - f(X^i)\|_2^2$$

$$\mathrm{MAE} = \frac{1}{N} * \sum_{i=1}^{N} \|Y^i - f(X^i)\|_1$$

Given these selections, the goal is to optimize the parameters of function $f(X)$ over the N input-output pairs.

$$f^*(X) = \min_{\mathrm{MSE/MAE}\ (W,\ b)} f(X)$$

We often wish to consider nonlinear functions in relating the inputs and outputs, and neural networks can express a useful collection of nonlinearities through compositions of layers or simple nonlinear functions. The rectified linear unit (ReLU)[21] is a popular component in neural networks;

$$y = \max(0, x) \qquad \text{(Rectified linear unit (ReLU))}$$

The nonlinear relation obtained by composing the linear function having weight matrix W_1 and bias vector b_1 with a rectified linear unit is

$$Y_1 = h(X) = \max(0, W_1 X + b_1)$$

A two-layered neural network can be formed by passing the output of previous relation through a linear transformation with weight matrix W_2 and bias vector b_2.

$$Y_2 = g(Y_1) = W_2 Y_1 + b_2$$
$$Y_2 = g(h(X)) = W_2 \max(0, W_1 X + b_1) + b_2$$

A three-layered neural network can similarly be formed with an additional weight matrix W_3 and bias vector b_3.

$$Y_3 = \tilde{f}(g(h(X))) = W_3 \max(0, W_2 \max(0, W_1 X + b_1) + b_2) + b_3$$

The preceding "fully connected" layers allow an arbitrary choice of weight matrices, and for image processing applications the optimization problems often are computationally infeasible. This issue was

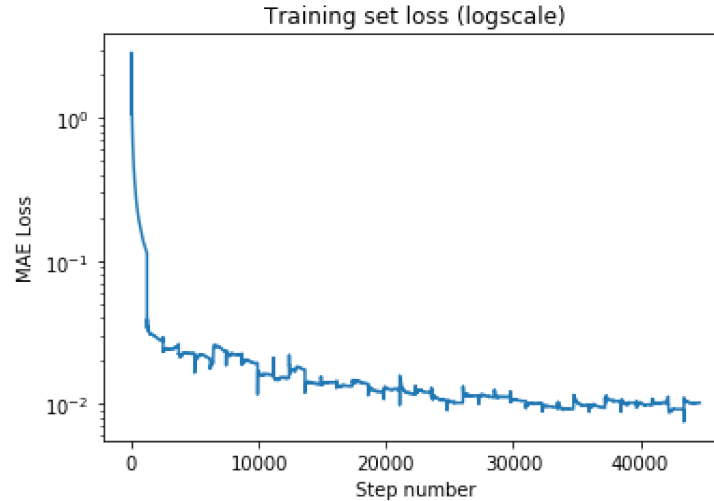

Figure 3. Training loss.

Table 1. Edge results for 1024 edge positions.

Original Image σ(nm), ξ(nm), α	Poisson noise level	Mean absolute error (pixels)	Left edge (nm) σ (true)	Left edge (nm) σ (observed)	Right edge (nm) σ (true)	Right edge (nm) σ (observed)	LWR (nm) (true)	LWR (nm) (observed)
0.8, 10, 0.3	2	0.61	0.75	0.71	0.74	0.66	1.06	0.95
0.8, 10, 0.3	5	0.40	0.75	0.73	0.74	0.67	1.06	0.97
0.8, 10, 0.3	10	0.22	0.75	0.75	0.74	0.72	1.06	1.04
0.8, 10, 0.3	100	0.01	0.75	0.75	0.74	0.74	1.06	1.06
1.2, 40, 0.7	2	0.44	1.06	1.06	1.21	1.23	1.41	1.42
1.2, 40, 0.7	5	0.27	1.06	1.06	1.21	1.22	1.41	1.42
1.2, 40, 0.7	10	0.15	1.06	1.08	1.21	1.21	1.41	1.42
1.2, 40, 0.7	100	0.01	1.06	1.06	1.21	1.21	1.41	1.42
1.6, 30, 0.5	2	0.69	1.56	1.53	1.59	1.46	2.34	2.23
1.6, 30, 0.5	5	0.38	1.56	1.57	1.59	1.52	2.34	2.28
1.6, 30, 0.5	10	0.23	1.56	1.57	1.59	1.59	2.34	2.33
1.6, 30, 0.5	100	0.01	1.56	1.56	1.59	1.58	2.34	2.33

addressed through the introduction of convolutional layers[22] in which the input and output of a layer can be represented by 3-dimensional tensors or volumes. A convolutional layer replaces a weight matrix with a set of filters with variable weights. The input tensor is convolved with these filters to generate an output tensor[23] with depth equal to the number of filters in the convolutional layer. Convolutional layers significantly reduce the number of weights in a layer and take advantage of the spatial information within images.

The depth of a neural network refers to the number of layers in the network.[21] Deeper networks can solve more complex tasks[14,21] because they incorporate more nonlinearities and can express more complex relationships. Deep convolutional neural networks underlie most recent success stories in machine learning[11,14,21,24] such as learning image features[11,14,21] in image classification problems, learning game states and strategies[24] in deep reinforcement learning problems and learning inverse problems like the denoising of images.[12,13] Multiple strategies have been developed to improve the training process and the accuracy of deep convolutional neural networks such as the development of better stochastic gradient descent[25,26] algorithms, the use of the ReLU nonlinearity[21] and the use of dropout[27] and batch-normalization[28] layers.

2.1 EDGENet

Our neural network EDGENet predicts two line edge positions from a 64x1024 noisy SEM image with pixel size 0:5x2 nm and containing one rough line as shown in Figure 1. The output of EDGENet is a 2-dimension matrix of size 2x1024 which contains the left and right edge positions of the line. EDGENet has seventeen convolutional layer with filter dimension of 3x3 and depth dimension equal to the depth of the input volume or tensor. The first four convolutional layers each have 64 filters, the next four convolutional layers each have 128 filters, the following four convolutional layers each have 256 filters and the subsequent four convolutional layers each have 512 filters. The last convolutional layer only has one filter. Figure 2 illustrates the output volume or tensor obtained after each convolutional layer.

In addition to these convolutional layers, EDGENet also applies one batch-normalization and one dropout layer after each of the first 16 convolutional layers. EDGENet has a total of 17 convolutional layers, 16 batch-normalization layers and 16 dropout layers. We selected dropout probability of 0.2 in all EDGENet dropout layers. EDGENet has 10,972,993 total parameters out of which 10,965,313 parameters

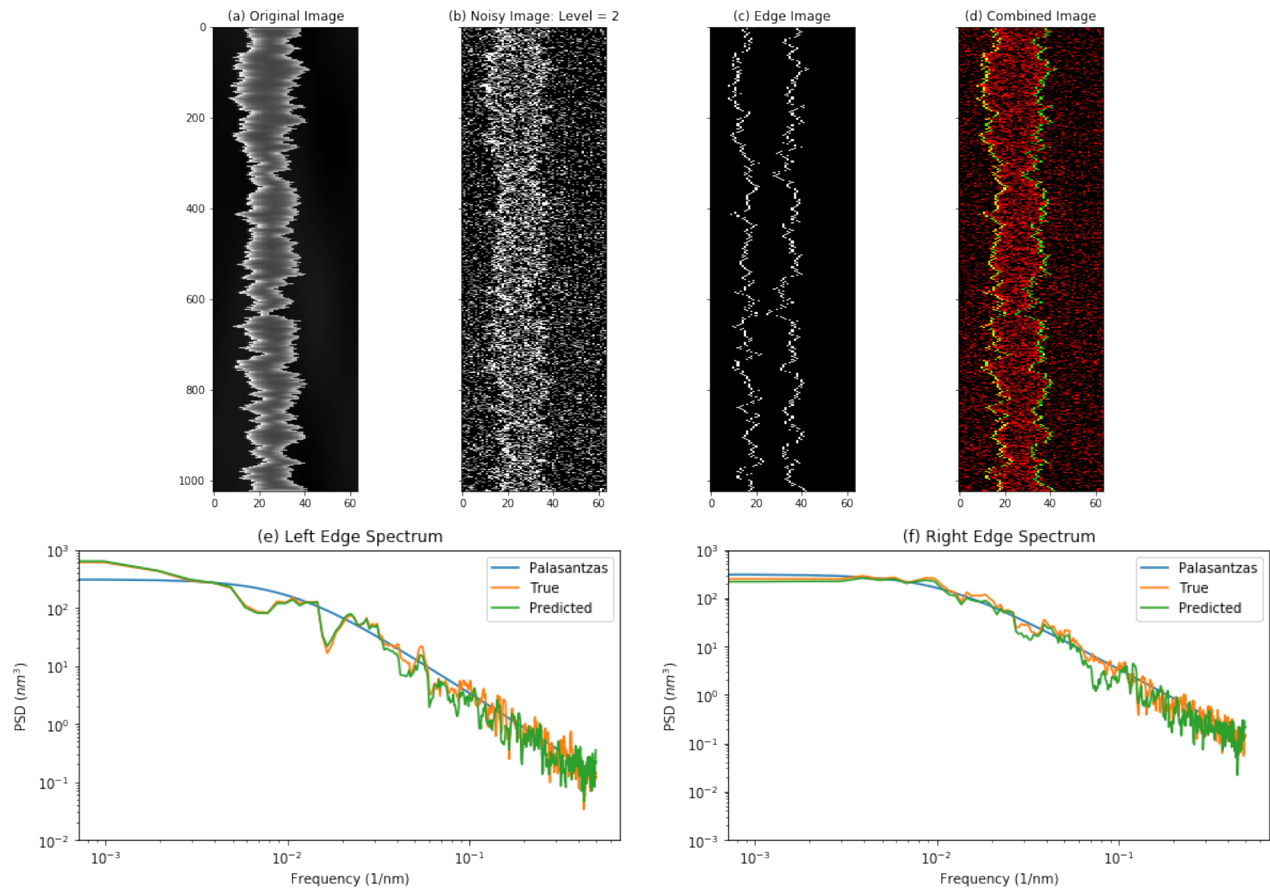

Figure 4. (a) Original image with σ = 1:6 nm, α = 0:5, ξ = 30 nm (b) Noisy image with a noise level of 2 electrons per pixels. (c) Predicted edge image. (d) Noisy image overlayed with edge image. (e) Left edge PSD; Palasantzas (blue), true edge (orange), predicted edge (green). (f) Right edge PSD; Palasantzas (blue), true edge (orange), predicted edge (green).

are trainable; the 7,680 non-trainable parameters are associated with the batch-normalization layers.

3. Simulation and Training Dataset

EDGENet applies the same set of 100800 noisy line images as SEMNet[15] for training and testing purposes. The edges each have length 2.048 microns, consist of 1024 pixels, and have an underlying Palasantzas spectral model. In the Palasantzas spectral model[18] the power spectral density (PSD) is denied by three parameters: the line edge roughness σ, the correlation length ξ and the Hurst/roughness exponent α.

$$PSD(f) = \frac{\sqrt{\pi}\Gamma(\alpha+0.5)}{\Gamma(\alpha)} \cdot \frac{2\sigma^2\xi}{(1+(2\pi f\xi)^2)^{\alpha+0.5}}$$

To construct a dataset with a wide variety of edge geometries we used eight choices for LER (σ = 0.4, 0.6, 0.8, 1.0, 1.2, 1.4, 1.6, 1.8 nm), nine choices of roughness/Hurst exponent (α = 0.1, 0.2, 0.3, 0.4, 0.5, 0.6, 0.7, 0.8, 0.9), and 35 choices of correlation length (ξ = 6, 7, ..., 40 nm). We used the Thorsos method[16,17] to generate eight edges for each combination of parameters and combined pairs of edges to create rough lines of widths 10 or 15 nanometers. These 10800 lines were input to NIST's SEM simulator ARTIMAGEN to generate images of dimension 64x1024 pixels with pixel size 0:5x2 nm. We added the artifacts of random backgrounds, a fixed edge effect, fine structure and Gaussian blur using the features of the ARTIMAGEN[19,20] simulator. We generated ten noisy images from each initial image by corrupting the latter with ten Poisson noise levels which are {2; 3; 4; 5; 10; 20; 30; 50; 100; 200} electrons per pixel. From this process, we formed a supervised learning dataset of noisy input images and output arrays of dimension 2x1024 with edge positions.

4. Experiments and Results

The simulated dataset was divided into a training set, a validation set and a test set. The test set consisted of the 8640 noisy SEM images and edge arrays with correlation length ξ in the set {10; 30; 40} nm. The validation set consisted of the 2880 noisy SEM images and edge arrays with correlation length ξ = 20 nm. The training set consisted of the remaining 89280 noisy SEM images with output edge arrays. EDGENet was trained with a Tesla K80 GPU and an Intel Xeon E5-2680 v4 2.40GHz node. EDGENet was created and trained using the Keras[29] library with the Tensorflow[30] library backend in the python programming language. We used a batch size of 8 noisy SEM images with edge arrays. All SEM image inputs and edge arrays were normalized to have values in the range (0,1). We chose the Adam[26] optimizer with a learning rate of 0.001 as our stochastic gradient descent algorithm. One epoch of training means running the stochastic gradient descent algorithms on the entire training set of 89280 noisy SEM images and edge arrays. EDGENet was trained for four epochs and the training time was approximately 45 hours and 30 minutes. We chose mean absolute error (MAE) as the loss function because it is better than

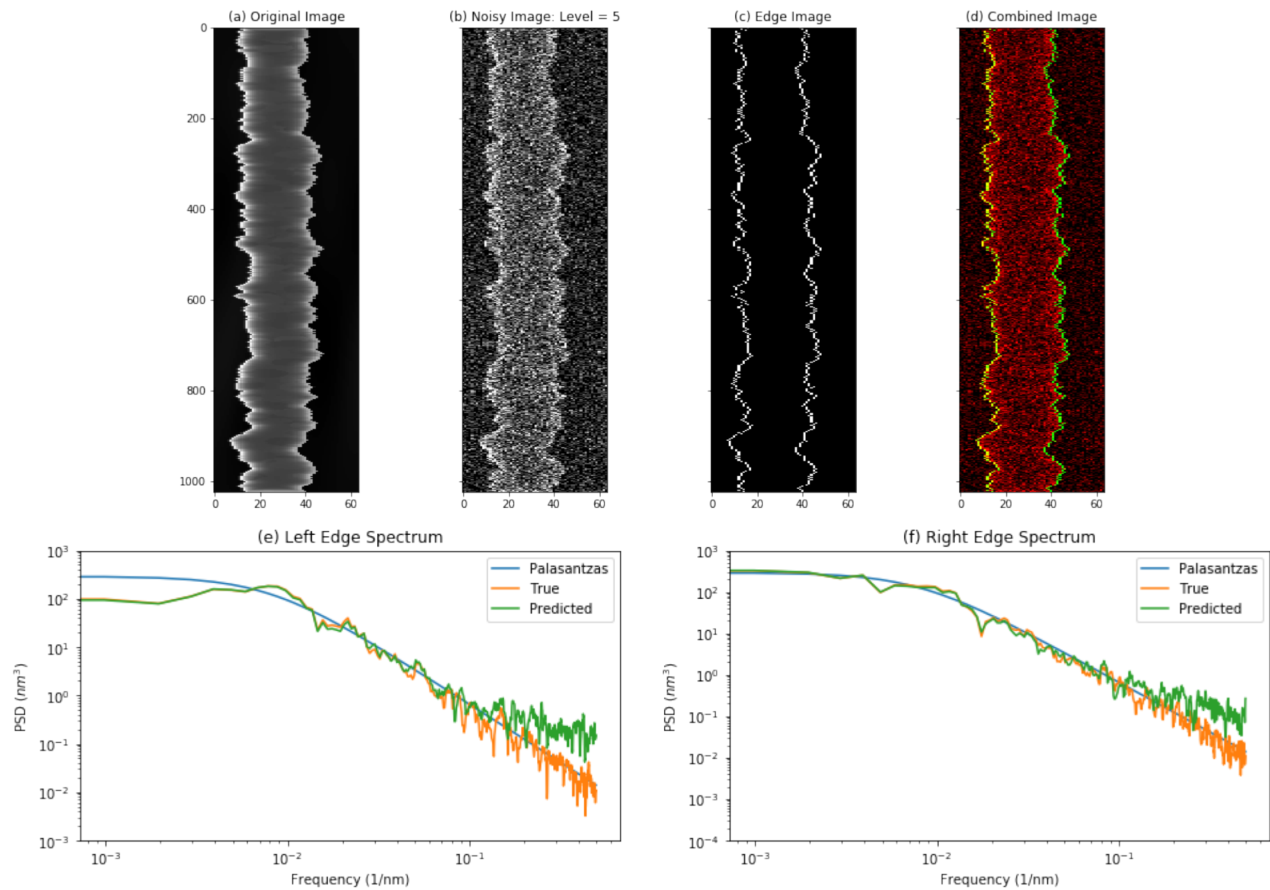

Figure 5. (a) Original image with σ = 1:2 nm, α = 0:7, ξ = 40 nm (b) Noisy image with a noise level of 5 electrons per pixels. (c) Predicted edge image. (d) Noisy image overlayed with edge image. (e) Left edge PSD; Palasantzas (blue), true edge (orange), predicted edge (green). (f) Right edge PSD; Palasantzas (blue), true edge (orange), predicted edge (green).

MSE in penalizing all edge position errors as opposed to large edge position errors.

Figure 3 plots the mean absolute error training loss as a function of the number of gradient descent steps in the Adam optimizer algorithm. The loss tends to decrease as the number of training steps increases. Further analysis of hyperparameters like the learning rate, the batch size and the number of epochs can potentially improve the training process. We saved the weights associated with the EDGENet model in a file of size 125 MB. This model le was later used to predict the line edge positions from the noisy SEM images in the test set. The average prediction time per image of EDGENet without including the time to load the model was approximately 2.4 seconds on a central processing unit.

We consider a few performance metrics to assess the quality of EDGENet on the test image dataset. Table 1 species three images and four Poisson noise levels and examines how these parameters affect the estimation of LER, LWR, and a metric from Ref. 15 named the mean absolute pixel error (MAE), which averages the absolute edge position estimation error measured in pixels over 2048 edge positions per line. Observe that even in the high noise regime the estimates of LER and LWR from the simulated test SEM images are very close to the true LER and LWR of the corresponding line from the edges generated through the Thorsos method. The mean absolute pixel error is close to zero in the low noise regime.

Figures 4-6 show additional results for three of the test images considered in Table 1. The edge images have been constructed from the edge positions predicted by EDGENet. We estimate the power spectrum from $N = 1024$ point edge positions using multitaper[31,32] spectrum estimation with six Slepian sequences, bandwidth W satisfying $NW = 4$, and adaptive weights. The resulting power spectral density (PSD) estimates for the edges generated from the Thorsos method and the corresponding predicted edges from the simulated test SEM images have been plotted together with the underlying Palasantzas power spectral density. Observe that for all three test images the predicted edge's PSD estimate closely matches the original edge's PSD estimate. For the first two test images the deviations from the Palasantzas PSD arise because we consider a single predicted edge per plot as opposed to the average of the multitaper estimates from multiple edges. The large difference between the Palasantzas PSD and the original and predicted edge PSD estimates in the low frequency regions of Figures 6(e) and 6(f) arise because the edge roughness parameter (0.8 nm) is close to the pixel width (0.5 nm).

5. Conclusion and Future Work

Deep supervised learning offers an effective method for finding the edge positions in SEM images corrupted by Poisson noise. The next step of this research is to predict nanostructure geometries from a larger class of SEM images. Since deep convolutional neural networks are effective at learning complex physical processes they have the potential to advance the field of semiconductor metrology.

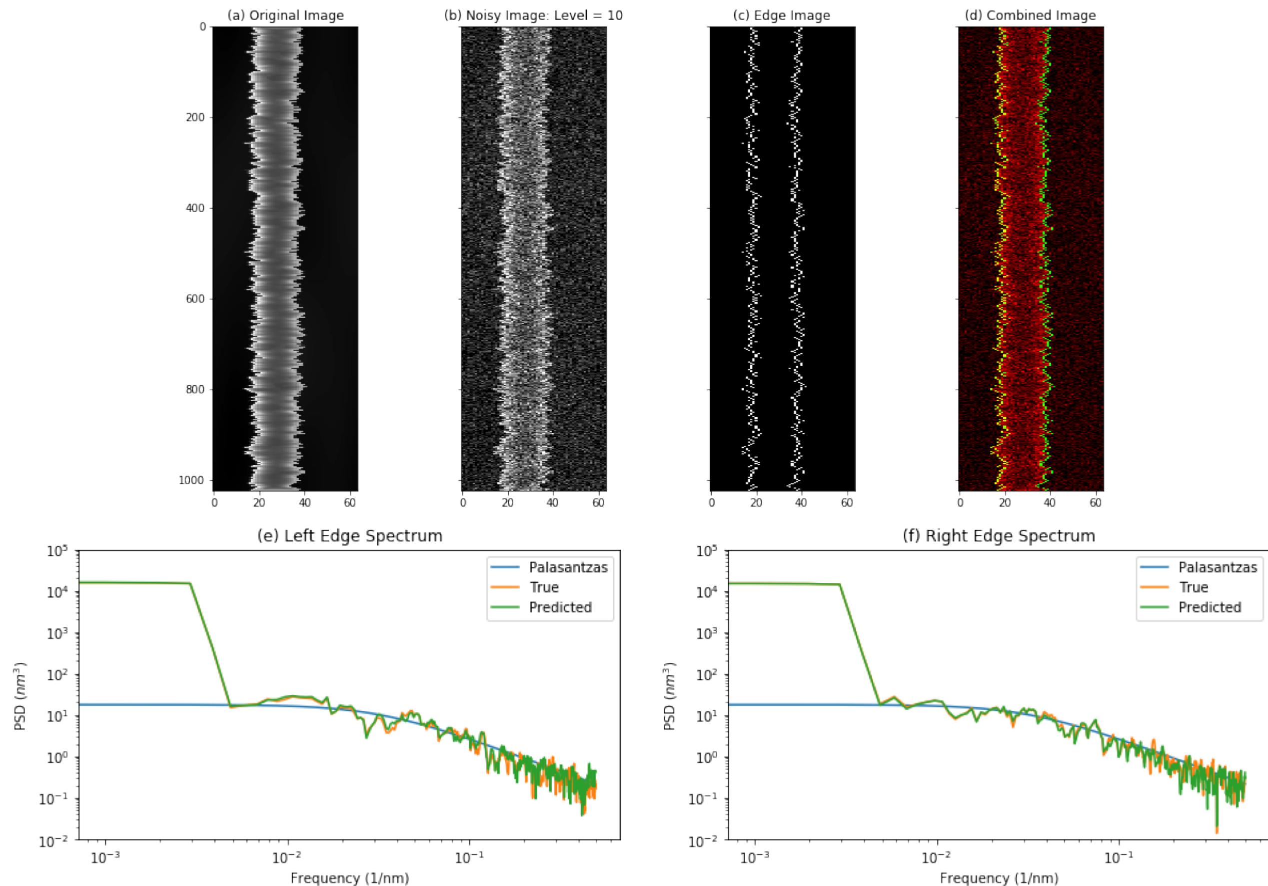

Figure 6. (a) Original image with σ = 0:8 nm, α = 0:3, ξ = 10 nm (b) Noisy image with a noise level of 10 electrons per pixels. (c) Predicted edge image. (d) Noisy image overlayed with edge image. (e) Left edge PSD; Palasantzas (blue), true edge (orange), predicted edge (green). (f) Right edge PSD; Palasantzas (blue), true edge (orange), predicted edge (green).

6. Acknowledgments

The authors used the Texas A&M University High Performance Research Computing Facility to conduct part of the research.

7. References

[1] Bunday, B. D., Bishop, M., McCormack, D. W., Villarrubia, J. S., Vladar, A. E., Dixson, R., Vorburger, T. V., Orji, N. G., and Allgair, J. A., "Determination of optimal parameters for CD-SEM measurement of line-edge roughness," in *Metrology, Inspection, and Process Control for Microlithography XVIII*, **Proc. of SPIE 5375,** 515-534, International Society for Optics and Photonics (2004).

[2] Villarrubia, J. S. and Bunday, B., "Unbiased estimation of linewidth roughness," in *Metrology, Inspection, and Process Control for Microlithography XIX*, **Proc. of SPIE 5752,** 480-489, International Society for Optics and Photonics (2005).

[3] Constantoudis, V., Patsis, G., Tserepi, A., and Gogolides, E., "Quantification of line-edge roughness of photoresists. ii. Scaling and fractal analysis and the best roughness descriptors," *Journal of Vacuum Science & Technology B: Microelectronics and Nanometer Structures Processing, Measurement, and Phenomena* **21**(3), 1019-1026 (2003).

[4] Mack, C. A. and Bunday, B. D., "Using the analytical linescan model for SEM metrology," in *Metrology, Inspection, and Process Control for Microlithography XXXI*, **Proc. of SPIE 10145,** 101451R, International Society for Optics and Photonics (2017).

[5] Verduin, T., Kruit, P., and Hagen, C. W., "Determination of line edge roughness in low-dose top-down scanning electron microscopy images," *Journal of Micro/Nanolithography, MEMS, and MOEMS* **13**(3), 033009 (2014).

[6] Mack, C. A., "Reducing roughness in extreme ultraviolet lithography," in *International Conference on Extreme Ultraviolet Lithography 2017*, **Proc. of SPIE 10450,** 104500P, International Society for Optics and Photonics (2017).

[7] Constantoudis, V., Papavieros, G., Lorusso, G., Rutigliani, V., Van Roey, F., and Gogolides, E., "Computational nanometrology of line-edge roughness: noise effects, cross-line correlations and the role of etch transfer," in *Advanced Etch Technology for Nanopatterning VII*, **Proc. of SPIE 10589,** 105890Y, International Society for Optics and Photonics (2018).

[8] De Simone, D., Rutigliani, V., Lorusso, G., De Bisschop, P., Vesters, Y., Carballo, V. B., and Vandenberghe, G., "EUV photoresist patterning characterization for imec N7/N5 technology," in *Extreme Ultraviolet (EUV) Lithography IX*, **Proc. of SPIE 10583,** 105830G, International Society for Optics and Photonics (2018).

[9] Chen, X., Verduijn, E., Wood, O., Brunner, T., Capelli, R., Hellweg, D., Dietzel, M., and Kersteen, G., "Evaluation of EUV mask impacts on wafer line-edge roughness using aerial and SEM image analyses (conference presentation)," in *Extreme Ultraviolet (EUV) Lithography IX*, **Proc. of SPIE 10583,** 105830J, International Society for Optics and Photonics (2018).

[10] Baravelli, E., Dixit, A., Rooyackers, R., Jurczak, M., Speciale, N., and De Meyer, K., "Impact of line-edge roughness on FinFET matching performance," *IEEE Transactions on Electron Devices* **54**(9), 2466-2474 (2007).

[11] LeCun, Y., Bengio, Y., and Hinton, G., "Deep learning," *Nature* **521**(7553), 436 (2015).

[12] Zhang, K., Zuo, W., Chen, Y., Meng, D., and Zhang, L., "Beyond a Gaussian denoiser: Residual learning of deep CNN for image denoising," *IEEE Transactions on Image Processing* **26**(7), 3142-3155 (2017).

[13] Jin, K. H., McCann, M. T., Froustey, E., and Unser, M., "Deep convolutional neural network for inverse problems in imaging," *IEEE Transactions on Image Processing* **26**(9), 4509-4522 (2017).

[14] He, K., Zhang, X., Ren, S., and Sun, J., "Deep residual learning for image recognition," in *Proceedings of the IEEE Conference on Computer Vision and Pattern Recognition*, 770-778 (2016).

[15] Chaudhary, N., Savari, S. A., and Yeddulapalli, S., "Deep supervised learning to estimate true rough line images from SEM images," *34th European Mask and Lithography Conference*. To appear in **Proc. of SPIE 10775** (2018).

[16] Mack, C. A., "Generating random rough edges, surfaces, and volumes," *Applied Optics* **52**(7), 1472-1480 (2013).

[17] Thorsos, E. I., "The validity of the Kirchho approximation for rough surface scattering using a Gaussian roughness spectrum," *The Journal of the Acoustical Society of America* **83**(1), 78-92 (1988).

[18] Palasantzas, G., "Roughness spectrum and surface width of self-affine fractal surfaces via the k-correlation model," *Physical Review B* **48**(19), 14472 (1993).

[19] Cizmar, P., Vladar, A. E., Ming, B., and Postek, M. T., "Simulated SEM images for resolution measurement," *Scanning* **30**(5), 381-391 (2008).

[20] Cizmar, P., Vladar, A. E., and Postek, M. T., "Optimization of accurate SEM imaging by use of artificial images," in *Scanning Microscopy 2009*, **7378**, 737815, International Society for Optics and Photonics (2009).

[21] Krizhevsky, A., Sutskever, I., and Hinton, G. E., "ImageNet classification with deep convolutional neural networks," in *Advances in Neural Information Processing Systems*, 1097-1105 (2012).

[22] LeCun, Y., and Bengio, Y., et al., "Convolutional networks for images, speech, and time series," *The Handbook of Brain Theory and Neural Networks* **3361**(10), 1995 (1995).

[23] Karpathy, A., "Stanford University cs231n: Convolutional neural networks for visual recognition," (2018).

[24] Silver, D., Schrittwieser, J., Simonyan, K., Antonoglou, I., Huang, A., Guez, A., Hubert, T., Baker, L., Lai, M., and Bolton, A., et al., "Mastering the game of Go without human knowledge," *Nature* **550**(7676), 354 (2017).

[25] Bottou, L., "Large-scale machine learning with stochastic gradient descent," in *Proceedings of COMP-STAT'2010*, 177-186, Springer (2010).

[26] Kingma, D. P. and Ba, J., "Adam: A method for stochastic optimization," *Proceedings of the 3rd International Conference on Learning Representations* (ICLR 2015) (2015).

[27] Srivastava, N., Hinton, G., Krizhevsky, A., Sutskever, I., and Salakhutdinov, R., "Dropout: A simple way to prevent neural networks from overfitting," *The Journal of Machine Learning Research* **15**(1), 1929-1958 (2014).

[28] Ioe, S. and Szegedy, C., "Batch normalization: Accelerating deep network training by reducing internal covariate shift," in *Proceedings of the 32nd International Conference on Machine Learning*, Bach, F. and Blei, D., eds., *Proceedings of Machine Learning Research* **37**, 448-456, PMLR, Lille, France (07-09 Jul 2015).

[29] Chollet, F. et al., "Keras." https://keras.io (2015).

[30] Abadi, M., Barham, P., Chen, J., Chen, Z., Davis, A., Dean, J., Devin, M., Ghemawat, S., Irving, G., Isard, M., Kudlur, M., Levenberg, J., Monga, R., Moore, S., Murray, D. G., Steiner, B., Tucker, P., Vasudevan, V., Warden, P., Wicke, M., Yu, Y., and Zheng, X., "Tensorflow: A system for large-scale machine learning," in *12th USENIX Symposium on Operating Systems Design and Implementation (OSDI 16)*, 265-283 (2016).

[31] Thomson, D. J., "Spectrum estimation and harmonic analysis," *Proceedings of the IEEE* **70**(9), 1055-1096 (1982).

[32] Luo, Y. and Savari, S. A., "Multitaper and multisegment spectral estimation of line-edge roughness," *Journal of Micro/Nanolithography, MEMS, and MOEMS* **16**(3), 034001 (2017).

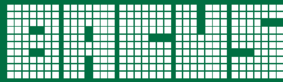

N • E • W • S

Sponsorship Opportunities

Sign up now for the best sponsorship opportunities

Photomask 2018 —
Contact: Melissa Farlow,
Tel: +1 360 685 5596; **melissaf@spie.org**

Advanced Lithography 2018 —
Contact: Teresa Roles-Meier,
Tel: +1 360 685 5445; **teresar@spie.org**

Advertise in the BACUS News!

The BACUS Newsletter is the premier publication serving the photomask industry. For information on how to advertise, contact:

Melissa Farlow,
Tel: +1 360 685 5596
melissaf@spie.org

BACUS Corporate Members

Acuphase Inc.
American Coating Technologies LLC
AMETEK Precitech, Inc.
Berliner Glas KGaA Herbert Kubatz GmbH & Co.
FUJIFILM Electronic Materials U.S.A., Inc.
Gudeng Precision Industrial Co., Ltd.
Halocarbon Products
HamaTech APE GmbH & Co. KG
Hitachi High Technologies America, Inc.
JEOL USA Inc.
Mentor Graphics Corp.
Molecular Imprints, Inc.
Panavision Federal Systems, LLC
Profilocolore Srl
Raytheon ELCAN Optical Technologies
XYALIS

Industry Briefs

Some Chipmakers Sidestep Scaling, Others Hedge

Ed Sperling

The rising cost of developing chips at 7nm coupled with the reduced benefits of scaling have pried open the floodgates for a variety of options involving new materials, architectures, and packaging that either were ignored or not fully developed in the past.

The economics of developing these devices is shifting. Multiple reports and analyses point to 3nm design costs topping $1 billion, and while the math is still speculative, there is no doubt that the cost per transistor or per watt is going up at each new node. That makes it hard for fabless chip companies to compete.

How these constantly evolving architectures get designed, manufactured, and packaged isn't entirely clear. What is clear is there is no shortage of new options emerging, and not all of them will work out. That makes it hard for foundries, equipment companies and materials suppliers to make long-range plans, which is why many are proceeding cautiously.

In the past, there was a roadmap and a clear direction for investing in the future of chip design through manufacturing. That roadmap no longer exists. Which approaches and technologies win, and which ones fail, is anyone's guess. But each one of those options requires a substantial investment, and it's hard to bet the bank when you don't know how long those options will stick around.

https://semiengineering.com/some-chipmakers-sidestep-scaling-others-hedge/

Automotive Electronic Systems to Grow 7% This Year and 6.3% Next Year, says IC Insights

David Manners

Sales of automotive electronic systems are forecast to increase 7.0% in 2018 and 6.3% in 2019, the highest growth rate in both years among the six major end-use applications for semiconductors, says IC Insights. Sales of automotive-related electronic systems are forecast to increase to $152 billion in 2018 from $142 billion in 2017, and are forecast to rise to $162 billion in 2019. Furthermore, automotive electronic systems are expected to enjoy a CAGR of 6.4% from 2017 through 2021, again topping all other major system categories, based on recent findings by IC Insights.

Technology features that are focused on self-driving (autonomous) vehicles, ADAS, vehicle-to-vehicle (V2V) communications, on-board safety, convenience, and environmental features, as well as ongoing interest in electric vehicles, continues to lift the market for automotive electronics systems, despite some highly publicized accidents involving self-driving vehicles this year that were at least partly blamed on technology miscues. New advancements are more widely available onboard mid-range and entry-level cars and as aftermarket products, which has further raised automotive system growth in recent years.

In the semiconductor world, this is particularly good news for makers of analog ICs, MCUs, and sensors since a great number of these devices are required in most of these automotive systems. It is worth noting that the Automotive—Special Purpose Logic category is forecast to increase 29% this year—second only to the DRAM market, and the Automotive—Application-Specific Analog market is forecast to jump 14% this year—as backup cameras, blind-spot (lane departure) detectors, and other "intelligent" systems are mandated or otherwise being added to more vehicles. Meanwhile, memory (specifically, DRAM and flash memory) is increasingly playing a more critical role in the development of new automotive system solutions used in vehicles.

https://www.electronicsweekly.com/news/business/automotive-electronic-systems-grow-7-year-6-3-next-says-ic-insights-2018-11/

Solution for Next Generation Nanochips Comes Out of Thin Air

Researchers at RMIT University have engineered a new type of transistor, the building block for all electronics. Instead of sending electrical currents through silicon, these transistors send electrons through narrow air gaps, where they can travel unimpeded as if in space.

The device unveiled in material sciences journal Nano Letters, eliminates the use of any semiconductor at all, making it faster and less prone to heating up.

Lead author and PhD candidate in RMIT's Functional Materials and Microsystems Research Group, Ms Shruti Nirantar, said this promising proof-of-concept design for nanochips as a combination of metal and air gaps could revolutionize electronics.

"Every computer and phone has millions to billions of electronic transistors made from silicon, but this technology is reaching its physical limits where the silicon atoms get in the way of the current flow, limiting speed and causing heat," Nirantar said.

Research team leader Associate Professor Sharath Sriram said the design solved a major flaw in traditional solid channel transistors – they are packed with atoms – which meant electrons passing through them collided, slowed down and wasted energy as heat.

"This is a step towards an exciting technology which aims to create something out of nothing to significantly increase speed of electronics and maintain pace of rapid technological progress," Sriram said.

https://electroiq.com/2018/11/solution-for-next-generation-nanochips-comes-out-of-thin-air/

Join the premier professional organization for mask makers and mask users!

About the BACUS Group

Founded in 1980 by a group of chrome blank users wanting a single voice to interact with suppliers, BACUS has grown to become the largest and most widely known forum for the exchange of technical information of interest to photomask and reticle makers. BACUS joined SPIE in January of 1991 to expand the exchange of information with mask makers around the world.

The group sponsors an informative monthly meeting and newsletter, BACUS News. The BACUS annual Photomask Technology Symposium covers photomask technology, photomask processes, lithography, materials and resists, phase shift masks, inspection and repair, metrology, and quality and manufacturing management.

Individual Membership Benefits include:

- Subscription to BACUS News (monthly)
- Eligibility to hold office on BACUS Steering Committee

www.spie.org/bacushome

Corporate Membership Benefits include:

- 3-10 Voting Members in the SPIE General Membership, depending on tier level
- Subscription to BACUS News (monthly)
- One online SPIE Journal Subscription
- Listed as a Corporate Member in the BACUS Monthly Newsletter

www.spie.org/bacushome

CALENDAR

2019

Photomask Japan
16-18 April 2019
PACIFICO Yokohama
Yokohama, Japan
www.photomask-japan.org

SPIE Advanced Lithography
24-28 February 2019
San Jose Marriott and
San Jose Convention Center
San Jose, California, USA

The 35th European Mask and Lithography Conference, EMLC 2019
17-19 June 2019
Hilton Hotel Dresden
Dresden, Germany

SPIE is the international society for optics and photonics, an educational not-for-profit organization founded in 1955 to advance light-based science, engineering, and technology. The Society serves nearly 264,000 constituents from 166 countries, offering conferences and their published proceedings, continuing education, books, journals, and the SPIE Digital Library in support of interdisciplinary information exchange, professional networking, and patent precedent. SPIE provided more than $4 million in support of education and outreach programs in 2017. **www.spie.org**

SPIE.

International Headquarters
P.O. Box 10, Bellingham, WA 98227-0010 USA
Tel: +1 360 676 3290
Fax: +1 360 647 1445
help@spie.org • **www.SPIE.org**

Shipping Address
1000 20th St., Bellingham, WA 98225-6705 USA

Managed by SPIE Europe
2 Alexandra Gate, Ffordd Pengam, Cardiff,
CF24 2SA, UK
Tel: +44 29 2089 4747
Fax: +44 29 2089 4750
spieeurope@spieeurope.org • **www.spieeurope.org**

You are invited to submit events of interest for this calendar. Please send to lindad@spie.org; alternatively, email or fax to SPIE.